SENTRI: Single-particle Energy Transducer for Radionuclide Injections for Personalized Targeted Radionuclide Cancer Therapy

Kyoungtae Lee Ph.D , Rahul Lall B.S , Shalini Chopra Ph.D , Michael J. Evans Ph.D , Michel M. Maharbiz Ph.D , Youngho Seo Ph.D , Mekhail Anwar M.D, Ph.D

PII: S0360-3016(23)08191-9
DOI: https://doi.org/10.1016/j.ijrobp.2023.11.057
Reference: ROB 28587

To appear in: *International Journal of Radiation Oncology, Biology, Physics*

Received date: 15 March 2023
Revised date: 11 August 2023
Accepted date: 27 November 2023

Please cite this article as: Kyoungtae Lee Ph.D , Rahul Lall B.S , Shalini Chopra Ph.D , Michael J. Evans Ph.D , Michel M. Maharbiz Ph.D , Youngho Seo Ph.D , Mekhail Anwar M.D, Ph.D , SENTRI: Single-particle Energy Transducer for Radionuclide Injections for Personalized Targeted Radionuclide Cancer Therapy, *International Journal of Radiation Oncology, Biology, Physics* (2023), doi: https://doi.org/10.1016/j.ijrobp.2023.11.057

SENTRI: Single-particle Energy Transducer for Radionuclide Injections for Personalized Targeted Radionuclide Cancer Therapy

Short running title: A mm-Scale *in vivo* Dosimeter for TRT

Author Names

1. **Kyoungtae Lee, Ph.D**
   - Department of Radiation Oncology, the University of California, San Francisco
   - Department of Electrical Engineering and Computer Science, Daegu Gyeongbuk Institute of Science and Technology
2. **Rahul Lall, B.S.**
   - Department of Electrical Engineering and Computer Science, the University of California, Berkeley
3. **Shalini Chopra, Ph.D**
   - Department of Radiology and Biomedical Imaging, the University of California, San Francisco
4. **Michael J. Evans, Ph.D**
   - Department of Radiology and Biomedical Imaging, the University of California, San Francisco
5. **Michel M. Maharbiz, Ph.D**
   - Department of Electrical Engineering and Computer Science, the University of California, Berkeley
6. **Youngho Seo, Ph.D**
   - Department of Radiology and Biomedical Imaging, the University of California, San Francisco, the University of California, San Francisco
7. **Mekhail Anwar, M.D, Ph.D**
   - Department of Radiation Oncology, the University of California, San Francisco
   - Department of Electrical Engineering and Computer Science, the University of California, Berkeley

Michel M. Maharbiz and Youngho Seo contributed equally to this work.

Corresponding Author

Kyoungtae Lee
+82-10-2270-9770
E3-512, Techno jungang-daero, Hyeonpung-eup, Dalseong-gun, Daegu, Republic of Korea. 42988
ktlee@berkeley.edu

Mekhail Anwar
(415)-514-2070
1825 Fourth St., First Floor, Room L1101, San Francisco, CA 94158

Mekhail.Anwar@ucsf.edu

Statistical Analysis Author

Kyoungtae Lee
+82-10-2270-9770
E3-512, Techno jungang-daero, Hyeonpung-eup, Dalseong-gun, Daegu, Republic of Korea. 42988
ktlee@berkeley.edu

Conflict of Interest

Michel M. Maharbiz is a co-CEO of iota Biosciences, Inc., a subsidiary of Astellas Pharma (However, no overlap in business interests or projects). Michel M. Maharbiz and Mekhail Anwar have a patent (US201662359672P) related to *in vivo* radiation sensing. No other potential conflicts of interest relevant to this article exist.

Funding

This work is supported by the following sources.
1. National Institutes of Health grant DP2DE030713 (M.A.)
2. National Science Foundation DGE2146752 (R.L.)
3. National Cancer Institute grant R01CA258297 (M.J.E.)
4. Congressionally Directed Medical Research Programs grant W81XWH-21-1-0498 (M.J.E.)
5. American Cancer Society grant 130635-RSG-17-005-01-CCE (M.J.E)
6. 2020 Challenge Award from the Prostate Cancer Foundation (M.J.E)
7. Benioff Institute for Prostate Cancer Research (M.J.E)
8. Precision Imaging of Cancer and Therapy Program at UCSF (M.J.E)

Acknowledgement

The authors would like to thank Zhang Hui for the preparation of mice with tumors.

A Data Sharing Statement

Research data are not available at this time

Abstract

Introduction: Targeted radionuclide therapy (TRT), whereby a tumor-targeted molecule is linked to a therapeutic beta- or alpha-emitting radioactive nuclide, is a promising treatment modality for patients with metastatic cancer, delivering radiation systemically. However, patients still progress due to suboptimal dosing, driven by the large patient to patient variability. Therefore, the ability to continuously monitor the real-time dose deposition in tumors and organs at risk (OARs) provides an additional dimension of

information during clinical trials that can enable insights into better strategies to personalize TRT.

Methods: Here, we present a single beta-particle sensitive dosimeter consisting of a 0.27 mm^3 monolithic silicon chiplet, directly implanted into the tumor. To maximize the sensitivity and have enough detection area, minimum size diodes (1 μm^2) are arrayed in 64×64. Signal amplifiers, buffers, and on chip memories are all integrated in the chip. For verification, PC3-PIP (PSMA+) and PC3-flu (PSMA-) cell lines are injected into the left and right flanks of the mice, respectively. The devices are inserted into each tumor, measure activities at 5 different time points (0-2 hour, 7-9 hour, 12-14 hour, 24-26 hour, and 48-50 hour) post ^{177}Lu-PSMA-617 injections. SPECT/CT scans are used to verify measured data.

Result: With a wide detection range from 0.013 to 8.95 MBq/mL, the system is capable of detecting high tumor uptake, as well as low doses delivered to OARs in real time. The measurement data is highly proportional ($R^2 > 0.99$) to the ^{177}Lu-PSMA-617 activity. The *in vivo* measurement data agrees well with the SPECT/CT results within acceptable errors (±1.5 %ID/mL).

Conclusion: Given the recent advances in clinical use of TRT in prostate cancer, the proposed system is verified in a prostate cancer mouse model using ^{177}Lu-PSMA-617.

Introduction

Radiotherapy is highly effective in treating cancer; however delivery of radiotherapy using conventional external beam radiotherapy (EBRT) to treat widespread metastatic disease is limited due to dose delivered to normal tissues, and the logistics of treating many sites of disease. Moreover, it is challenging to treat all sites of metastatic disease using EBRT since microscopic pockets of disease are not visible under diagnostic imaging. Molecularly targeted radionuclide therapy (TRT) enables systemic delivery of radiation through the chelation of radioactive isotopes with tumor-specific ligands. The radiopharmaceuticals circulate inside the body, attach to cancer cells, and emit radiation, damaging nearby (from microns to millimeters, depending on the radionuclide) cells. The goal of TRT is to deliver a sufficient dose over multiple treatment cycles within tumors to ablate cancer cells, while minimizing unwanted dose deposition to organs at risk (OARs), such as the kidneys, salivary glands, bladder, and radiosensitive bone marrow.

TRT has shown promise in the treatment of metastatic castrate resistant prostate cancer (mCRPC), and has redefined treatment in metastatic cancer. For example, ^{177}Lu, as therapeutic radionuclide, is chelated to small molecular ligands that bind to prostate-specific membrane antigen (PSMA), a cell surface enzyme over-expressed in prostate cancer cells (1). Recently the US Food and Drug Administration (FDA) approved ^{177}Lu-PSMA-617 TRT for patients with mCRPC has demonstrated ~35 % improvement in overall survival, but patients still progress at a median 8.7 months after treatment (2). On this basis, developing strategies to augment the therapeutic impact of TRTs is an urgent unmet need.

Although TRT has successfully shown its applicablity in prostate and neuroendocrine cancer, there is still significant variation in patient response (3). Many patients still progress, reflecting potential suboptimal dosing for a subset of patients. Moreover, the dose limits for OARs such as kidneys with TRT are still being determined requiring accurate knowledge of OAR dose for each patient. Variability in delivered dose to the tumor and OARs can be attributed to factors including but not limited to 1) tumor-specific antigen expression; 2) ligand internalization, retention, and off rate; 3) biodistribution, which varies as a function of blood flow, heart rate, and excretion kinetics; and 4) uptake on OARs. However, despite these patient-specific variations, the current clinical standard of care is to dose each patient identically over a set number of cycles. Therefore, improved understanding of the delivered dose to the tumors and OARs could yield additional insight into patient-specific dose response, both in terms of tumor dose and control as well as OAR dose and toxicity. This information may inform the optimal subsequent doses of TRT for each patient.

Given that TRT is delivered in multiple serial doses, there is an opportunity to adapt dosing at subsequent cycles based on the prior dosimetry to achieve a critical threshold dose for tumors. Several clinical trials are currently exploring the possibility of adaptive dosing strategies to improve treatment efficacy (ClinicalTrials.gov Identifier : NCT02754297, NCT04917484, and NCT05896371). Several results reported in literature exploring individualized dosing have shown a significant improvement in treatment response (e.g., prostate-specific antigen level, progression-free survival, and overall survival) in ^{177}Lu-based therapy for patients undergoing maximum dose escalation to the tumor (e.g., until the total kidney or bone marrow dose was maximized to the safety limit) (4, 5). Other researchers have modulated the

fractionation schedule based on the treatment response (e.g., prostate-specific antigen level and image-based dosimetry) to the initial standard administration (6). Therefore, dosimetry-based personalized TRT has shown promise in improving the treatment outcome and therefore garnered interest in clinical trials further exploring better personalized dosing strategies.

The current state-of-the-art dosimetry uses a single timepoint single-photon emission computed tomography (SPECT) scan to provide an accurate whole-body snapshot of the delivered dose to tumors and OARs at a given time point. Because of the aforementioned patient heterogeneity, individual time-activity curves have been shown to have variations in t_{max} (the time to maximum uptake) and T_{eff} (the time it takes for the dose in organs to become half) as high as 50 % and 30 %, respectively (3). Multi-time point SPECT/CT scans can provide more complete time course data, however they present a logistical challenge and the most common approach is to use a single-time point SPECT/CT combined with the time-activity curve. SPECT/CT-based time-activity curve estimation is usually done by curve-fitting of time-activity curve models, meaning more data points, ideally continuously acquired data, can mathematically provide better datasets and basis functions compared to one or a few SPECT/CT scans. Here, we present proof-of-concept of a novel device that is synergistic with SPECT/CT that enables direct measurement of radiation activity in tissue with high temporal resolution over long time scales. This platform has the potential to provide an additional dimension of information during clinical trials to enable new strategies to personalize TRT (Fig. 1A and B).

Our approach is to directly measure the continuous activity inside of tissue using millimeter-scale dosimeters implanted in tissue. To enable *in vivo* dosimetry for personalized TRT, these dosimeters must 1) be millimeter-scale for minimizing the foreign body reaction and implanting using a core biopsy needle; 2) have a wide dynamic range to accurately measure the dose uptake that can span from <1 %ID/mL for OARs to ~20 %ID/mL for tumors in real-time, and 3) consume sub-mW electrical power for battery or wireless power transfer requirements. Despite the efforts toward *in vivo* dosimetry, no previous works have satisfied all those requirements (7–13). Most works focused on the measurement of x-rays during external beam radiotherapy or brachytherapy, and to the best of the authors` knowledge, there has been no prior published work on using implantable dosimetry for TRT.

To maximize sensitivity and obviate the need for bulky external readout equipment, here we present a proof-of-concept diode-based sub-millimeter scale (0.94×0.96×0.3 mm^3) single beta-particle sensitive custom integrated circuit (IC) dosimeter, which we call SENTRI (Single-particle Energy Transducer for Radionuclide Injections). By exploiting a complementary metal oxide transistor (CMOS) fabrication technology, all the required electrical signal amplification and processing circuitry to operate the diode detectors are integrated into a monolithic silicon chiplet (Fig. 1C). The proposed system does not require bulky external equipment; only sub-mW electrical power (0.5 mW) and digital data acquisition (< 4 kbps) are necessary. In addition, the proposed IC-based SENTRI platform enables **continuous, real-time dose measurement by directly counting** the number of beta-particles incident on the SENTRI chip. The sensor response is quantified in counts per minute (CPM), the total detected hits over the entire chip per minute. We demonstrate the first *in vivo* verification result for ^{177}Lu-PSMA-617 in animal models using human prostate cancer cell lines.

Materials and Methods

Designing a 64×64 diode-based *in vivo* dosimeter silicon chip

Reversely biased P-N diodes form a depletion region between P and N-type silicon. Incident beta-particles penetrating through the depletion region deposit energy (E_{dep}), generating electron-hole-pairs (EHPs) (Fig. 1D). The number of EHPs (n_{EHP}) is proportional to the particle's linear energy transfer (LET), which is nonlinearly dependent on the particle energy (14). These generated electrons are integrated onto the parasitic capacitance, C_{int}, creating a voltage drop, V_{drop} ($V_{drop} = q_e n_{EHP}/C_{int}$). Since V_{drop} is inversely proportional to C_{int}, smaller diodes, which have smaller parasitic capacitances, provide higher sensitivity. Therefore, by exploiting the miniaturization inherent in CMOS fabrication technology, we shrink the diode to a nearly minimum size (1 μm^2). See Fig. S1 and note for the diode size optimization and E_{dep} calculation. To obtain sufficient counts for statistical accuracy, the P-N diodes are arranged in a 64×64 array, resulting in a detection area and fill factor of 512×512 μm^2 and 1/64, respectively.

All necessary signal amplification, data processing, and on-chip memory circuitry are integrated on a SENTRI chip (Fig.S3). Each pixel consists of a P-N diode, signal amplifier, filter, buffers, and 1-bit

static random-access memory (SRAM). Due to variations during fabrication, there are pixel-to-pixel variations even with 'identical' pixels, resulting in differences in pixel offset and gain that render the pixels non-functional. We implement in-pixel SRAM to selectively disable any of these non-functional pixels. The total size of each pixel, including in-pixel circuitry, is 8×8 μm^2. The SENTRI chip measures $0.96\times0.94\times0.3$ mm^3 and consumes static power of ~0.5 mW. A minimal ~10 μm silicon dioxide layer on the diodes, inherent in the CMOS fabrication process, minimizes energy loss from incident beta particles while protecting the chip from the biofluid penetration.

The SENTRI chip is bonded on a flexible printed circuit board (FPCB). UV-curable epoxy is applied to protect wires and exposed areas of the FPCB with care to leave the detection area exposed to maximize sensitivity (Fig. 1E). The final packaged sensor has a width of 6 mm and thickness of <1 mm. An external motherboard provides electrical power and digital communication between the SENTRI chip and laptop. A custom python-based script running on the laptop communicates with the motherboard.

^{177}Lu-PSMA-617 radiolabeling

$^{177}LuCl_3$ is purchased from Oak Ridge National Laboratory. A stock solution of PSMA-617 (Vipivotide tetraxetan, MedChemExpress) is first prepared in dimethyl sulfoxide (DMSO) with a concentration of 1mg/mL. For radiolabeling, 185 MBq of $^{177}LuCl_3$ is transferred to a reaction vial. The pH of the solution is adjusted to 6 by adding 100 μL ammonium acetate (0.2M solution). Then, 25 μg of PSMA-617 is added to the reaction solution. The reaction is allowed to occur at 50°C with constant shaking for 45 minutes.

The radiolabeled solution is checked for labeling efficiency by performing thin layer chromatography (TLC) on a Whatman 41 paper as a stationary phase and 20 mM citric acid as a mobile phase. The TLC strip is scanned on the TLC reader (AR-2000, Bioscan).

^{177}Lu-PSMA-617 is purified using a SEP-PAK Plus C8 cartridge. The cartridge is preconditioned with 5mL ethanol (100%) and 5 mL water. The reaction solution is pushed through the C8 cartridge and waste (unlabeled ^{177}Lu) is collected in a vial. ^{177}Lu-PSMA-617 is eluted with 2 mL ethanol solution (100%). Ethanol is evaporated under a vacuum with a constant flush of N_2 at 40ºC. Dried ^{177}Lu-PSMA-617 is reconstituted in a formulation of DMSO:Tween 80:saline (10%:10%:80% v/v) before injections for mice.

***In vivo* measurements**

All protocols and procedures are approved by the Institutional Animal Care and Use Committee (IACUC) of XXXXX (anonymized for review). All animal research follows the National Institutes of Health (NIH) guidelines, described in the Guide for the Care and Use of Laboratory Animals.

Fig. 2A depicts procedures for the *in vivo* experiment. 4-week-old homozygous athymic male mice (N=15) are used for this study. 2.5 million PC3-PIP and PC3-flu cells are subcutaneously injected into the left and right flanks of the mice, respectively. When the tumor reaches a proper size for experiments (~17 days after the cancer cell injection), 15 mice are randomly divided into 5 groups for each time point; 0-2 hour, 7-9 hour, 12-14 hour, 24-26 hour, and 48-50 hour post-injection. Surgery is performed on 0-2 hour time point mice and a ~10 minute measurement is conducted before the ^{177}Lu-PSMA-617 injection. The remaining mice are administered ^{177}Lu-PSMA-617 first, with the surgery and measurement being performed when they reach the desired time point. About 200 μL of ^{177}Lu-PSMA-617 solution is slowed injected through the tailvein. Fig 2B shows an experiment photo.

The mouse is anesthetized with 2.5 % isoflurane and 1.5 L/min oxygen flow. Each tumor is carefully cut (~1 cm depth and width) using a surgical blade. Then, each device is inserted into the tumor and connected to the mainboard. The activity of each tumor is measured for 2 hours. Then, the mouse is sacrificed and transported to the SPECT/CT bed for image acquisition. With the devices still in each tumor, the SPECT/CT machine (VECTor4CT, MILabs) scans the whole body for 30 minutes with the energy detection range from 0 to 1.2 MeV using a 3.6 mm pinhole collimator. After the SPECT/CT scan, the devices are taken out from the animal.

Converting measured CPM into %ID/mL

One week after the animal experiment, all devices measure three different ^{177}Lu-PSMA-617 concentrations to compensate for the device-to-device variation. Concentrations are determined so that recorded CPM from the animal measurement by each device is within the 3-point calibration range. The linear regression is performed on the data set measured by each device. Finally, the decay-corrected %ID/mL value of the animal experiment is calculated as below.

$$\%ID/mL_{meas} = 100 \times \frac{CPM - b}{a \times inj} \times e^{\lambda t_{inj}},$$

where CPM is the mean CPM value of the last 30 minutes of the animal measurement, a and b are the slope and y-intercept of the linear regression curve, respectively, inj is the injected ^{177}Lu-PSMA-617 activity in MBq, λ is a decay constant of ^{177}Lu, and t_{inj} is the time difference between the injected time and measured time in hours.

Results

Measuring a wide range of ^{177}Lu concentrations

The system is first characterized using 10 different concentrations of ^{177}Lu-PSMA-617 in saline solution. The ^{177}Lu concentration ranges from 0.013 to 8.95 MBq/mL (corresponding to 0.06~40 %ID/mL assuming 22 MBq injection in a mouse), matching the therapeutic range in mice model (15). The SENTRI chip is submerged in the solution, from the lowest to highest concentration, and measures the signal for ~1 hour (Fig. 3A). The sensor response is quantified in counts per minute (CPM), the total detected hits over the entire chip per minute. Fig. 3B shows transient CPM plots for various ^{177}Lu concentrations. Fluctuations in CPM is mainly due to the Poisson nature of radioactive decay.

The measured mean CPM is highly proportional to the ^{177}Lu concentrations with R^2 value greater than 0.99 (Fig. 3C), demonstrating a wide dynamic range. No saturation on CPM is observed. The relative errors, defined as the percentage error between the measurement and linear fit, ranges from -3.23 to 1.99 %.

To observe any long-term sensitivity degradation or fluid penetration disrupting sensor operation, the SENTRI chip is submerged in 8.88 MBq/mL ^{177}Lu-PSMA-617 with saline solution and continuously measures the activity for 35 days (Fig. 3D). The measured counts per hour (black dots) shows an exponential decay and matches well with both the theoretical decay curve (the dotted red curve, with t_{half} = 6.7 days) and gamma counter measurement results (red diamonds, acquired using Hidex Automatic Gamma Counter). The error, defined as the difference between the normalized counts per hour and theoretical value, is within ±0.05, and no sensitivity degradation or device malfunction is observed.

***In vivo* verification**

As shown in Fig. 4, the SENTRI chips are visible under a CT scan. Fig. 5 shows the measured transient plots for PC3-PIP and PC3-flu at each time point. As shown in the leftmost plot (0-2 hour post-injection), there is zero signal recorded before the injection. The CPM increases in both tumors immediately after the injection. The 7-9 hour post-injection mice have the highest CPM in the PC3-PIP tumor. After the peak PSMA-617 uptake, the CPM within the PC3-PIP tumors gradually decreases until 52 hours post-injection. At all time points, CPM in PC3-PIP is significantly higher than that in PC3-flu, corresponding to the PSMA overexpression in the PC3-PIP model. The measured PC3-flu activity is highest during 0-2 hour post-injection and rapidly decreases over time, representing dose to an OAR.

3-point calibration to convert CPM into %ID/mL

To account for device-to-device variations introduced in manufacturing, we use a 3-point calibration method to find the relationship between CPM and %ID/mL for each SENTRI chip. Fig. 6A shows a 3-point calibration measurement result for a SENTRI chip that measured M6 (7-9 hour time point) PC3-PIP tumor. A linear regression line between the concentration and CPM is shown in solid red. The uncertainty of the slope a and y-intercept b are ±0.58 and ±0.045, respectively. Finally, using the linear regression line, the CPM value from the mice measurements is converted into the %ID/mL value.

Fig. 6B depicts normalized histograms of a and b for all SENTRI chips used in mouse experiments (30 in total). The mean and standard error of a and b are 27.09±4.88 CPM/(MBq/mL) and 0.13±0.22 CPM, respectively. The variations in a and b are primarily due to device-to-device mismatches which can be calibrated prior to the actual measurement. Note that the b values are close to 0, demonstrating that the system inherently has zero offset, an issue for other types of *in vivo* dosimeters (9–11). The variation in height of the wirebonds and epoxy contributes to the variation in a.

The decay-corrected uptake curves of the last 30 minutes of each measurement in PC3-PIP and PC3-flu tumors across all mice are shown in Fig. 6C. The trends in the uptake curves match well with the previously reported trends, a linear and mono-exponential decay for PC3-PIP, and a mono-exponential decay for PC3-flu (3). The ratio between %ID/mL values in PC3-PIP and PC3-flu tumors are lowest at the

initial time point (1.1×) and highest at 7-9 hour time point (193×), modeling the therapeutic ratio between the tumor and OAR in a clinical setting.

Comparison of SENTRI with SPECT/CT

Finally, measured %ID/mL values are compared with SPECT/CT imaging results. To account for tumor heterogeneity (inherent in centimeter-scale mouse tumors) and the finite distance that emitted beta-particles travel (mean = ~0.3 mm, range = 0-1.7 mm), only the surrounding 1 mm of tissue is used for comparison to SPECT/CT. Mean %ID/mL values in the 2 mm diameter sphere region of interest (ROI) from the Gaussian-filtered SPECT/CT images are plotted. The ROI is placed at the location of the SENTRI chip. The absolute %ID/mL errors ($\%ID/mL_{SENTRI}$ - $\%ID/mL_{SPECT}$) in all mice are within ±1.5 %ID/mL, showing agreement with the SPECT/CT results. The relationship between $\%ID/mL_{SENTRI}$ and $\%ID/mL_{SPECT}$ is highly linear in both PC3-PIP and PC3-flu tumors with R^2 values of 0.95 and 0.78, respectively (Fig.7A and B). Additionally, a Bland-Altman plot for comparing measurements between SENTRI and SPECT/CT is shown in Fig.7C. The difference in %ID/mL has a mean and standard deviation of 0.12 and 0.54 %ID/mL, respectively. The errors are due to imperfect measurement and limited spatial resolution in SPECT/CT scans. Gaussian post-filtering of the SPECT/CT scans adds uncertainty, particularly when the tumor is heterogeneous. See supplementary Fig. S2 and note for SPECT/CT calibration and Gaussian post-filtering. In addition, unequal spill-in and spill-out effects, a distortion generated in an image due to the finite full width half maximum of a point spread out function, in the SPECT/CT scan can be another source of error on a small scale.

Discussion

Here, we have demonstrated proof-of-concept that the radiation activity can be measured using a millimeter-scale implantable dosimeter with single particle sensitivity over long time courses. SENTRI successfully measured various concentrations (0.06~40 %ID/mL) of ^{177}Lu-PSMA-617 activity with high linearity ($R^2 > 0.99$). SENTRI was successfully implanted and measured continuous activity over 2 hours in PC3-PIP and PC3-flu prostate cancer cell lines grown in mice. To better validate the sensor as a measure of activity, each sensor was subjected to titration of ^{177}Lu-PSMA-617 and using this calibration,

the measured CPS in the tumor was converted to %ID/mL value. This activity derived from the sensor matched very closely the activity determined by SPECT/CT for the same animal.

SENTRI is ideally suited for continuous measurement of TRT activity in tissue. Using this information, one potential application is to synergistically integrate SENTRI data with single time point SPECT/CT to gain a fuller understanding of the total integrated dose within each patient. This may allow for personalized adaptation of either (or both) the subsequent doses for each cycle of the treatment, or the number of cycles. For example, the SENTRI chip measures the real-time activity at a single location over multiple half-life, and by integrating these two datasets, it may be possible to extrapolate the integrated dose in tumors and OARs over long time courses (3, 16).

Although we chose ^{177}Lu-PSMA-617 for verification because it is FDA-approved and widely used in practice, the fundamental technological achievement opens the door for the use of the proposed system for other types of antibodies, small molecules, or peptides (i.e. ^{177}Lu-DOTATATE), and for cancer types beyond prostate (17, 18). Since the SENTRI chip directly measures radiation, we believe this system can be utilized for nearly all types of radioligands, potentially not only personalizing treatment but also helping characterize new radioligands by providing continuous uptake curves. In addition, the proposed system can also personalize alpha-particle-based TRTs, such as the ones using ^{225}Ac or ^{227}Th, which have recently gained popularity since they deposit much larger energy within a small distance. However, SPECT/CT dosimetry for alpha-emitting TRTs is challenging because of the significantly lower administered dose, and hence fewer gamma-particles, requiring a longer SPECT/CT acquisition time (19).

In order for the system to be utilized in clinical settings, a number of technical challenges must be addressed. Given short travel length of beta-particles in tissue, SENTRI is subject to tumor heterogeneity, reporting only the local environment in which it is implanted. In our mouse models, for proper device implantation, the tumor size needs to be greater than ~1 cm, relatively large for a mouse and thus often has a significant heterogeneity. However, this is a small tumor in a patient. Tumor heterogeneity can be addressed by implanting multiple SENTRI sensors in a single tumor (often ~3 gold seed markers can be easily placed in a tumor), or by specifically placing SENTRI in a non-necrotic area of tumor, identified on a pretherapy PET scan. Next, the device must be fully wirelessly integrated. Given the power

consumption (< 0.6 mW) and data rate (107 bits per second at 8.95 MBq/mL) of the system, radio-frequency, ultrasound, or magnetoelectric methods are all well applicable (20–22). A transceiver antenna, rectifier, and modulator/demodulators are the only necessary components for wireless operation. Once a wireless interface is implemented, we can greatly reduce the overall size of the system. Lastly, long-term *in vivo* usage requires a more robust packaging (or coating) to prevent device degradation or failure due to biofluid penetration. The simplest solution would be using a thin (~50 μm) Parylene coating that lasts ~6 months, sufficient to cover all fractions (23). A ceramic packaging can be another option, as it provides more robustness and thus ensures longer operation (24, 25).

Conclusion

We successfully demonstrated the functionality of SENTRI in human prostate cancer small animal models. It is envisioned that the proposed system can be utilized to help personalize the TRT, significantly improving the overall safety and efficacy of the treatment through safe dose management.

References

1. Israeli, Ron, Powell, Thomas, Fair, William. Molecular Cloning of a Complementary DNA Encoding a Prostate-specific Membrane Antigen. *Cancer Research*. 1993;53:227–230.

2. Sartor O, de Bono J, Chi KN, *et al.* Lutetium-177–PSMA-617 for Metastatic Castration-Resistant Prostate Cancer. *N Engl J Med*. 2021;385:1091–1103.

3. Peters SMB, Hofferber R, Privé BM, *et al.* [68Ga]Ga-PSMA-11 PET imaging as a predictor for absorbed doses in organs at risk and small lesions in [177Lu]Lu-PSMA-617 treatment. *Eur J Nucl Med Mol Imaging*. 2022;49:1101–1112.

4. David Mirando, Yuni Dewaraja, Alexandria Kruzer, *et al.* Personalized therapy planning for 177Lu-DOTATATE using a kidney-driven dose optimization method. *J Nucl Med*. 2019;60:270.

5. Sandström M, Garske-Román U, Granberg D, *et al.* Individualized Dosimetry of Kidney and Bone Marrow in Patients Undergoing ^{177} Lu-DOTA-Octreotate Treatment. *J Nucl Med*. 2013;54:33–41.

6. Emmett L, John N, Pathmanandavel S, *et al.* Patient outcomes following a response biomarker-guided approach to treatment using 177Lu-PSMA-I&T in men with metastatic castrate-resistant prostate cancer (Re-SPECT). *Ther Adv Med Oncol*. 2023;15:175883592311563.

7. Beyer GP, Mann GG, Pursley JA, *et al.* An Implantable MOSFET Dosimeter for the Measurement of Radiation Dose in Tissue During Cancer Therapy. *IEEE Sensors J.* 2008;8:38–51.

8. Bloemen-van Gurp EJ, Haanstra BKC, Murrer LHP, *et al.* In Vivo Dosimetry With a Linear MOSFET Array to Evaluate the Urethra Dose During Permanent Implant Brachytherapy Using Iodine-125. *International Journal of Radiation Oncology*Biology*Physics*. 2009;75:1266–1272.

9. Andersen CE, Nielsen SK, Greilich S, *et al.* Characterization of a fiber-coupled Al2O3:C luminescence dosimetry system for online *in vivo* dose verification during I192r brachytherapy: Fiber-coupled Al2O3:C luminescence dosimetry. *Med. Phys.* 2009;36:708–718.

10. Jursinic PA, Yahnke CJ. *In vivo* dosimetry with optically stimulated luminescent dosimeters, OSLDs, compared to diodes; the effects of buildup cap thickness and fabrication material: *In vivo* dosimetry with optically stimulated luminescent dosimeters. *Med. Phys.* 2011;38:5432–5440.

11. Wang LLW, Perles LA, Archambault L, *et al.* Determination of the quenching correction factors for plastic scintillation detectors in therapeutic high-energy proton beams. *Phys. Med. Biol.* 2012;57:7767–7781.

12. Zhuang Q, Yaosheng H, Yu M, *et al.* Embedded structure fiber-optic radiation dosimeter for radiotherapy applications. *Opt. Express*. 2016;24:5172.

13. Yorke E, Alecu R, Ding L, *et al. Diode in Vivo Dosimetry for Patients Receiving External Beam Radiation Therapy*. AAPM; 2005.

14. Anon. NIST Measured Electron Stopping Power Data.

15. Ruigrok EAM, van Vliet N, Dalm SU, *et al.* Extensive preclinical evaluation of lutetium-177-labeled PSMA-specific tracers for prostate cancer radionuclide therapy. *Eur J Nucl Med Mol Imaging*. 2021;48:1339–1350.

16. Wang J, Zang J, Wang H, *et al.* Pretherapeutic 68Ga-PSMA-617 PET May Indicate the Dosimetry of 177Lu-PSMA-617 and 177Lu-EB-PSMA-617 in Main Organs and Tumor Lesions. *Clin Nucl Med*. 2019;44:431–438.

17. Strosberg JR, Caplin ME, Kunz PL, *et al.* 177Lu-Dotatate plus long-acting octreotide versus high-dose long-acting octreotide in patients with midgut neuroendocrine tumours (NETTER-1): final overall survival and long-term safety results from an open-label, randomised, controlled, phase 3 trial. *The Lancet Oncology*. 2021;22:1752–1763.

18. Banerjee SR, Kumar V, Lisok A, *et al.* 177Lu-labeled low-molecular-weight agents for PSMA-targeted radiopharmaceutical therapy. *Eur J Nucl Med Mol Imaging*. 2019;46:2545–2557.

19. Seo Y. Quantitative Imaging of Alpha-Emitting Therapeutic Radiopharmaceuticals. *Nucl Med Mol Imaging*. 2019;53:182–188.

20. Piech DK, Johnson BC, Shen K, *et al.* A wireless millimetre-scale implantable neural stimulator with ultrasonically powered bidirectional communication. *Nat Biomed Eng*. 2020;4:207–222.

21. Chen JC, Kan P, Yu Z, *et al.* A wireless millimetric magnetoelectric implant for the endovascular stimulation of peripheral nerves. *Nat. Biomed. Eng*. 2022;6:706–716.

22. Shin G, Gomez AM, Al-Hasani R, *et al.* Flexible Near-Field Wireless Optoelectronics as Subdermal Implants for Broad Applications in Optogenetics. *Neuron*. 2017;93:509-521.e3.

23. Hassler C, Boretius T, Stieglitz T. Polymers for neural implants: Polymers for Neural Implants. *J. Polym. Sci. B Polym. Phys.* 2011;49:18–33.

24. Shen K, Maharbiz MM. Ceramic packaging in neural implants. *J. Neural Eng.* 2021;18:025002.

25. Shen K, Maharbiz MM. Design of Ceramic Packages for Ultrasonically Coupled Implantable Medical Devices. *IEEE Trans. Biomed. Eng.* 2020;67:2230–2240.

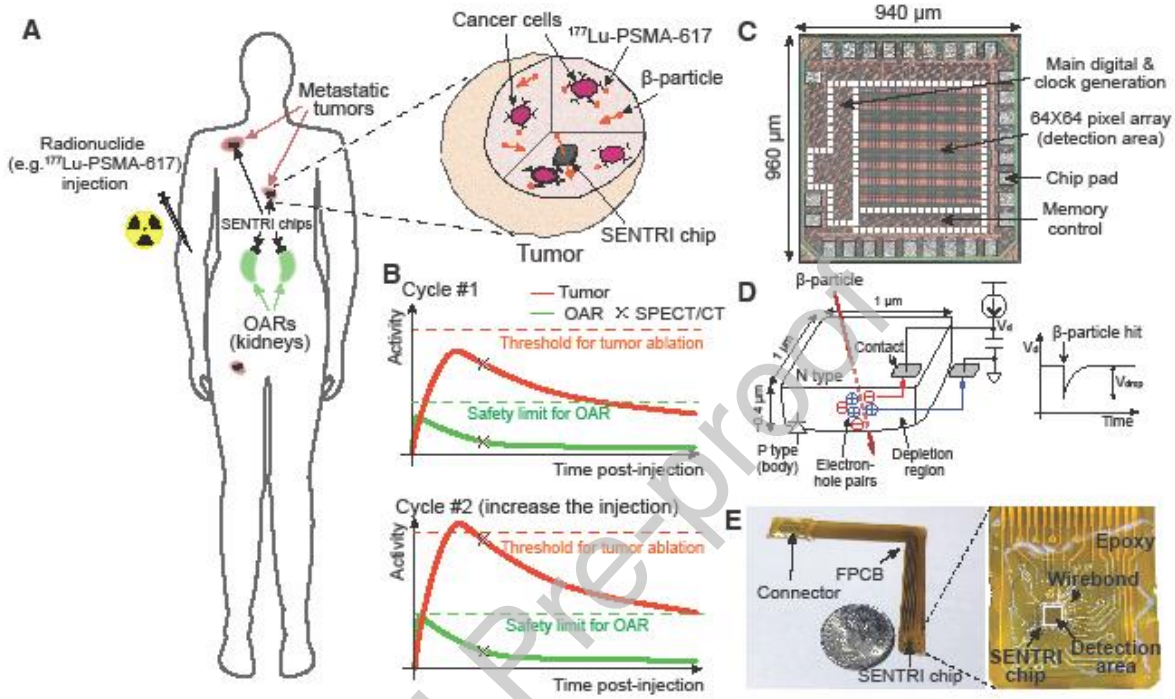

Figure 1 A Schematic view of the personalized in vivo dosimetry system for TRT. The proposed devices can monitor tumor and OAR (e.g. kidneys) uptake in real-time. Radionuclides attached on the cells emit beta-particles that are detected by SENTRI chip with single particle sensitivity. **B** An example of tumor and OAR uptake and dose planning strategy over multiple cycles. **C** Photograph of the SENTRI chip. 4,096 diodes as well as necessary circuitry are all integrated in a single chip. **D** Single beta-particle sensing scheme using an ultra-small (1 μm^2) P-N silicon diode. Generated electron-hole-pairs accumulate to a nearby capacitor, creating an instant voltage drop, V_{drop}. **E** Photograph of the SENTRI chip and FPCB with a Unites States dime for size comparison (left) and picture under a microscope (right).

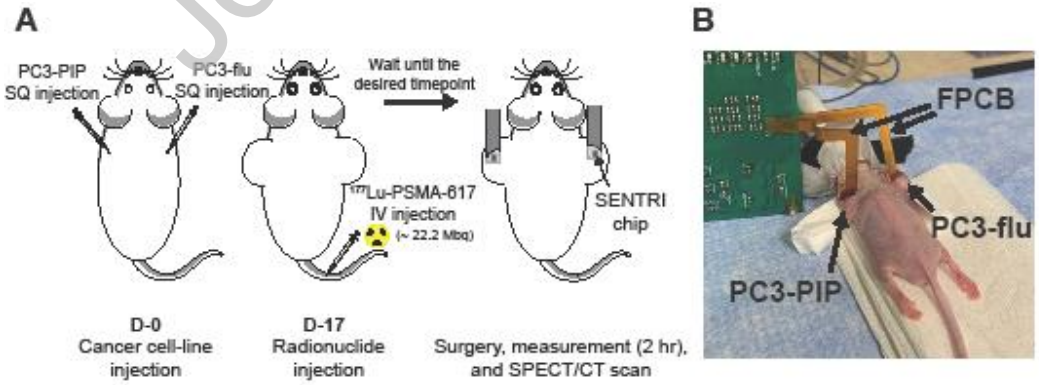

Figure 2 A. Schematic of the in vivo experiment. **B.** Photograph of the in vivo experiment.

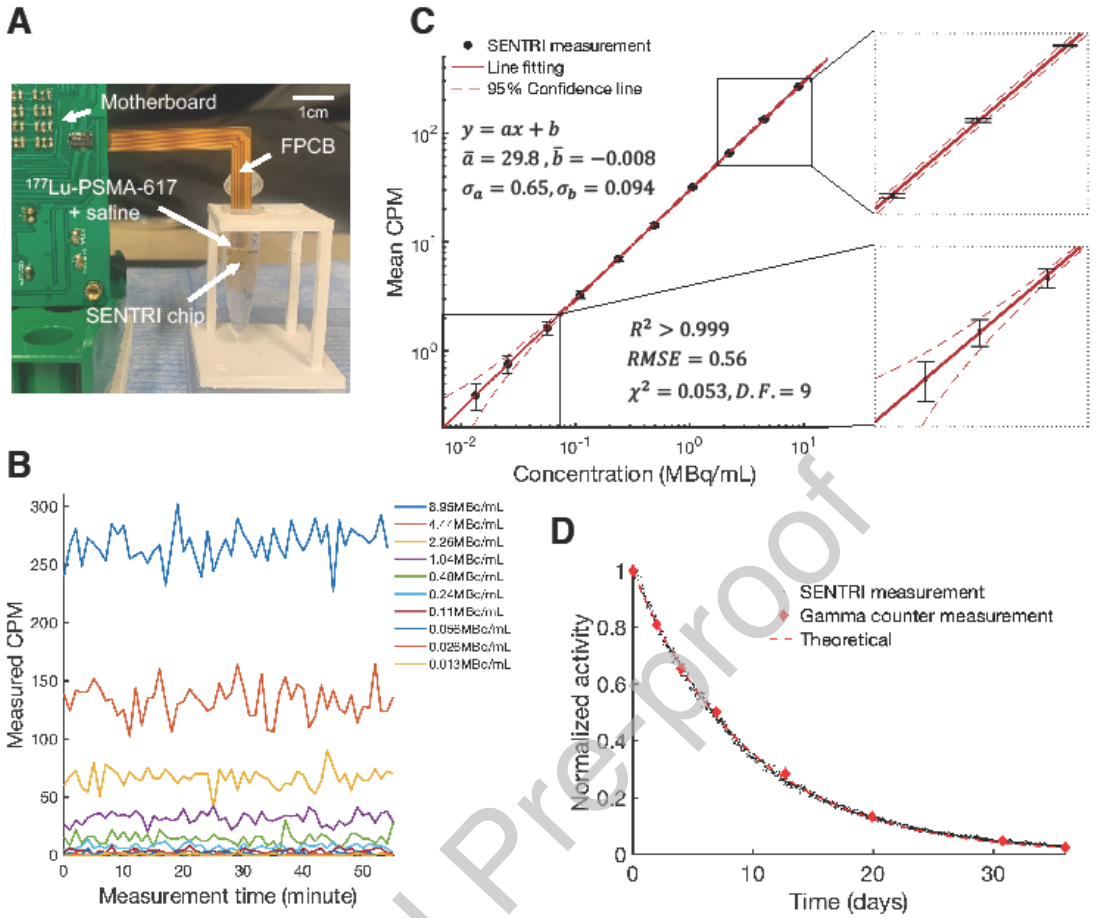

Figure 3 A. Photograph of the sensor characterization experiment. **B.** Recorded raw transient CPM for various ^{177}Lu concentrations. **C.** ^{177}Lu concentration vs. mean CPM log scale plot with a least relative error linear regression and 95 % confidence range. Zoomed in plots are shown on the right. **D.** Long-term measurement results.

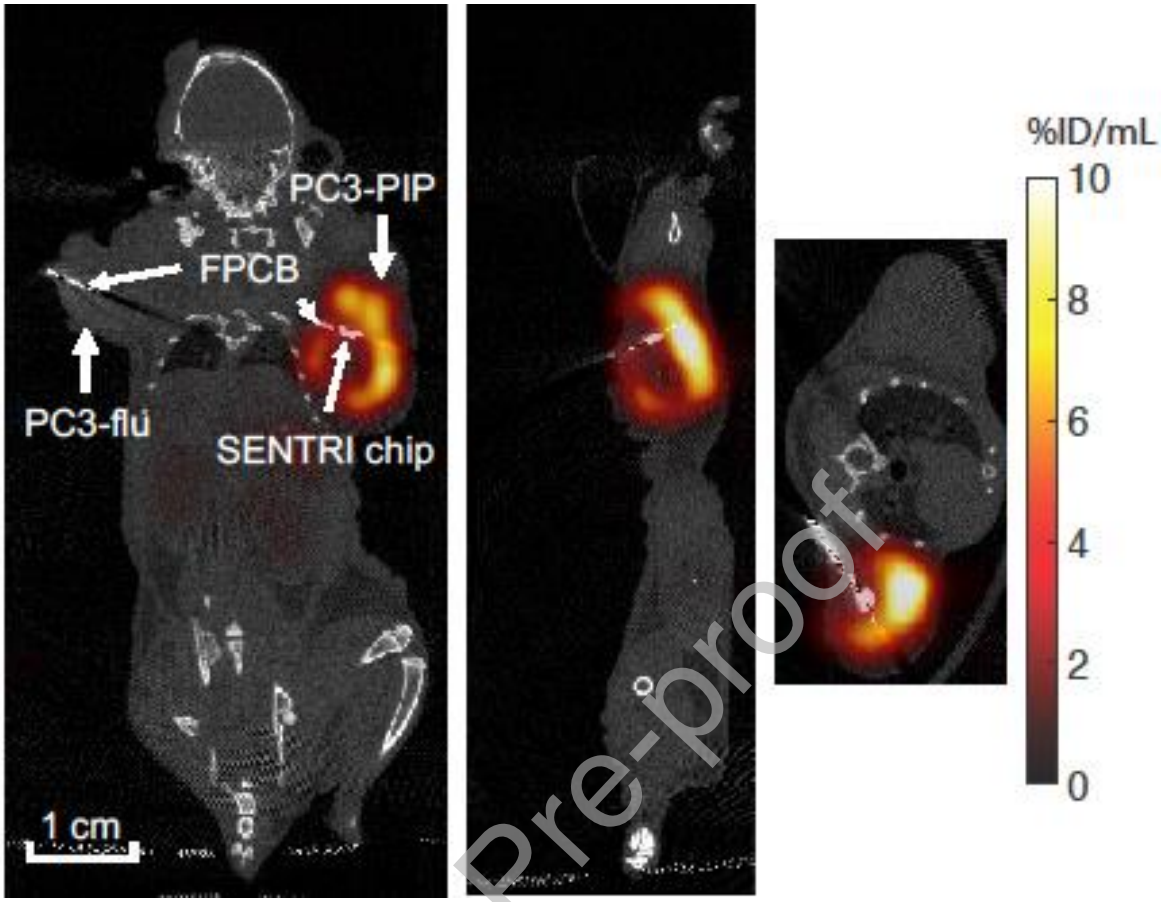

Figure 4 Coronal (left), sagittal (middle), and transverse (right) Gaussian-filtered SPECT/CT images of M6 (7-9 hour time point).

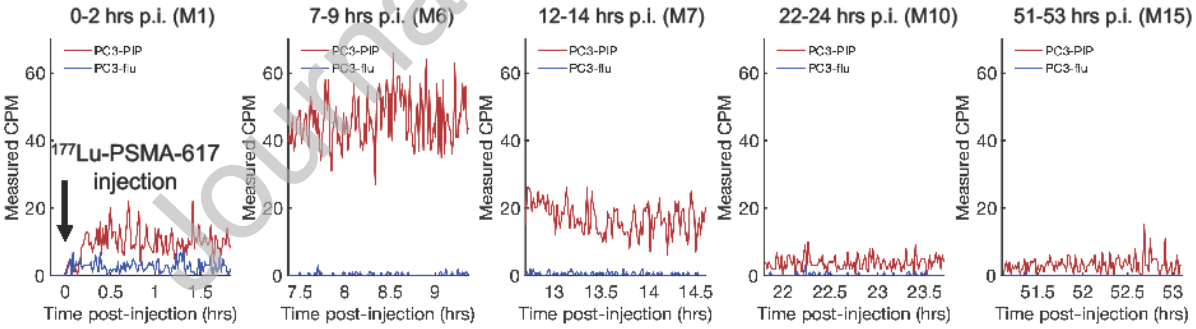

Figure 5 Measured transient CPM curves for PC3-pip (red) and flu (blue) at various time points.

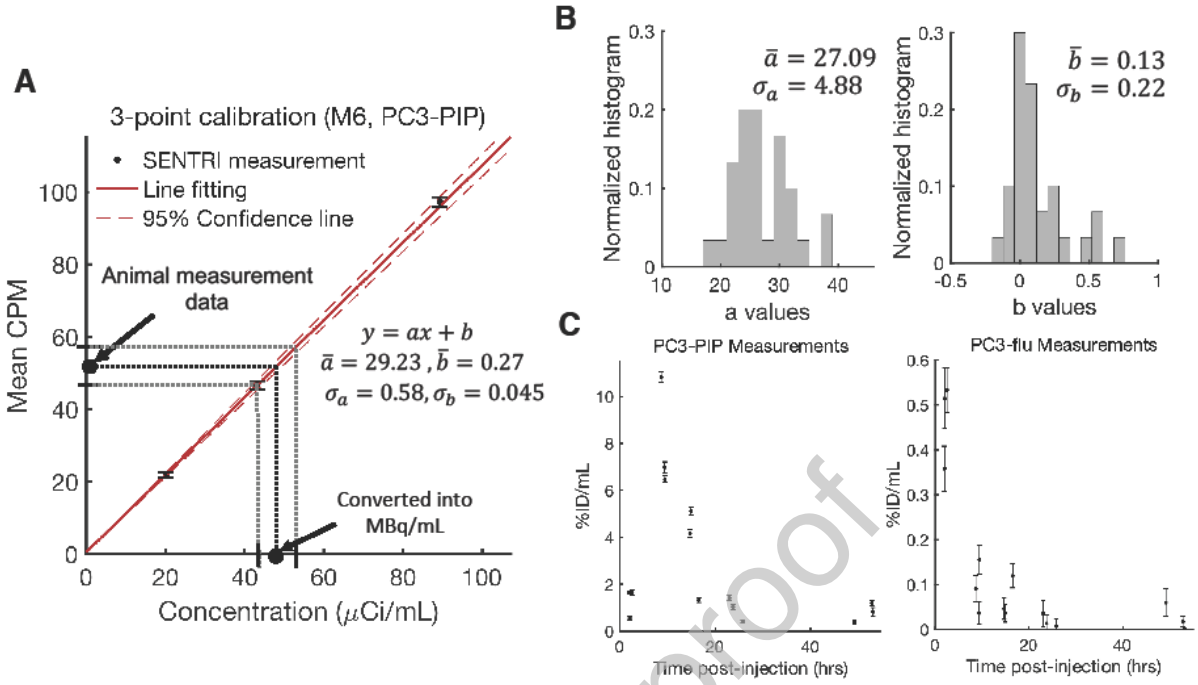

Figure 6 A. A 3-point calibration result for a device that measured M8 (7-9 hour time point) PC3-PIP tumor. **B.** Histograms of the slope a (left) and y-intercept b (right) for all devices.

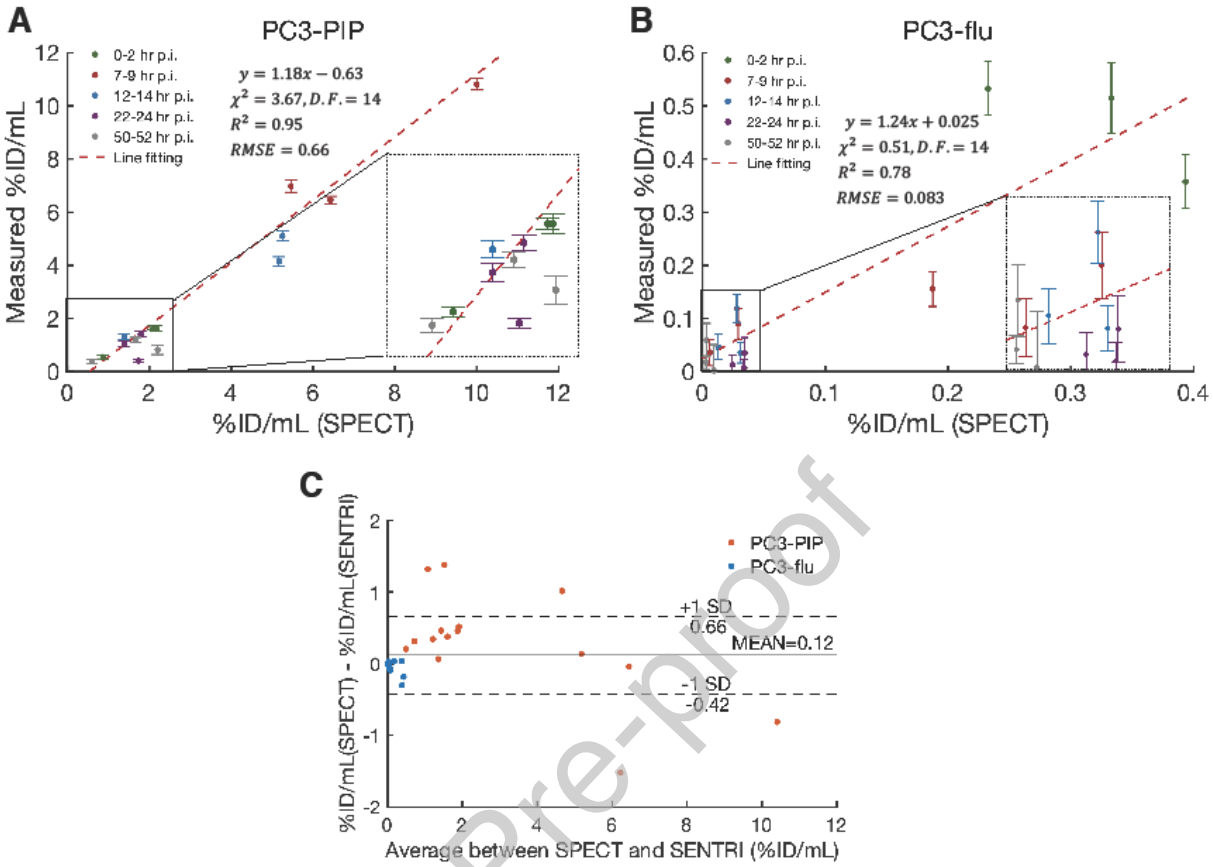

Figure 7 %ID/mL from SPECT (x-axis) vs. measured %ID/mL (y-axis) plots with zoomed in images for PC3-PIP (**A**) and flu (**B**). Linear regression line (dotted red) is displayed. Each data point is color coded by time points. **C** A Bland-Altman plot comparing SENTRI and SPECT/CT measured %ID/mL.